Band structure sensitive photoresponse in twisted bilayer graphene proximitized with WSe_2

Aparna Parappurath,[1,*] Bhaskar Ghawri,[1] Saisab Bhowmik,[2] Arup Singha,[1] K. Watanabe,[3] T. Taniguchi,[4] and Arindam Ghosh[1,5,†]

[1] *Department of Physics, Indian Institute of Science, Bangalore, 560012, India*
[2] *Department of Instrumentation and Applied Physics, Indian Institute of Science, Bangalore, 560012, India*
[3] *Research Center for Functional Materials, National Institute for Materials Science, Namiki 1-1, Tsukuba, Ibaraki 305-0044, Japan*
[4] *International Center for Materials Nanoarchitectonics, National Institute for Materials Science, Namiki 1-1, Tsukuba, Ibaraki 305-0044, Japan*
[5] *Centre for Nano Science and Engineering, Indian Institute of Science, Bangalore 560 012, India*

I. DEVICE FABRICATION AND MEASUREMENT METHODS

A. Device fabrication

The heterostructure was assembled using the well-known 'tear and stack' method. Individual flakes of single layer graphene, hexagonal Boron nitride (hBN), and Tungsten diselenide (WSe_2) were exfoliated on Si^{++}/SiO_2 wafer and identified using an optical microscope. A hemispherical stamp of polydimethylsiloxane (PDMS) coated with Polypropylene carbonate (PPC) film was used for picking up the individual layers. Using the sharp edge of hBN, the single layer of graphene is torn, and the two separated sheets of graphene are manually rotated to 1.2° to make angle controlled tBLG stack.

The thickness of hBN(18 nm) and WSe_2(∼3-4 nm corresponds to 3-4 layer thickness [1–3]) was confirmed using Atomic Force Microscopy(Fig.S1a). Raman spectroscopy is employed to characterize Single layer graphene (Fig.(S1b)). Adding the hBN layer helps passivate trap states/impurities and ripples from the SiO_2 layer. By encapsulating the devices with hBN, the extrinsic effects from polymers during the fabrication process could also get minimized. Furthermore, spin-orbit coupling and associated effects in tBLG is expected to be influenced by the number of WSe_2 layer. However, we do not see the effect of WSe_2 in our transport measurements as the minimum experimental temperature is limited to 12 K. In this work, the role of WSe_2 is to act as a photon-absorbing layer. The number of WSe_2 layers can affect photon absorption efficiency. It would also determine the electric field drop across the flake.

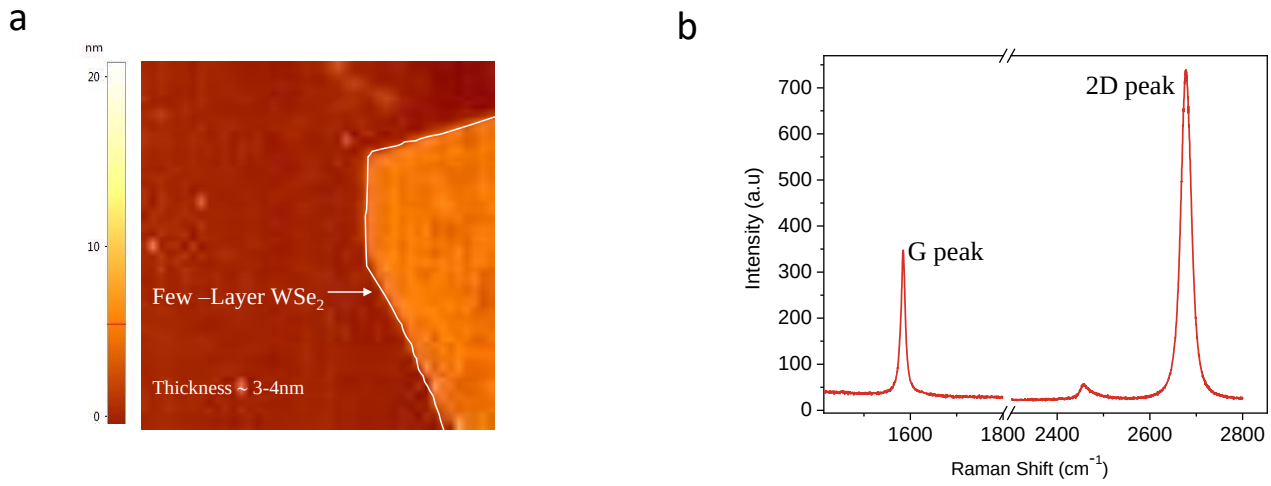

Fig. S1. Characterization of **(a)** WSe_2 layer using AFM and **(b)** Single layer graphene using Raman spectroscopy measurements

B. Optoelectronic Measurements

Electrical and Optoelectronic measurements were performed in a cryogen-free, pumped Montana cryostat with an optical window to couple the light. The photoresponse measurements were performed using well calibrated commercial LEDs, illuminated on device through a collimating optical window. All transport measurements were performed with a bias current of 100 nA, using an SR830 low-frequency lock-in amplifier at 226 Hz. The number density in the system was tuned using the global Si^{++}/SiO_2 back gate.

II. DISCUSSION ON FLAT BANDS IN WSe_2 PROXIMITIZED $tBLG$

The emergence of the flat bands near the magic angle can be understood qualitatively from the competition between the kinetic energy and the interlayer hybridization energy. Intuitively, when the hybridization energy is comparable to or larger than the kinetic energy of the moiré superlattice cell, the two layers are hybridized strongly, and the lower of the hybridized states is pushed to and crosses zero energy, leading to isolated low-energy flat bands[4] . However, the exact calculation showing the emergence of flat bands requires detailed mathematical formulation solving the Hamiltonian of the coupled system and has already been shown previously in multiple reports[5, 6]. It is also to be noted that, the band structure calculations in magic-angle tBLG have demonstrated a substantial asymmetry between the conduction and valence bands. For example, the bandwidth and magnitude of the superlattice gap can vary upon changing the type of carriers. Although the strength of electron-electron interactions and band gaps can alter when a transition metal dichalcogenide (TMDC) layer is placed on tBLG, the electron-hole asymmetry in the system does not change significantly [7].

III. BAND FILLING FACTOR AND TWIST ANGLE ESTIMATION

Band filling factor 'ν' is obtained by the standard approach that has been followed conventionally in tBLG literature [4, 7, 8]). With the applied gate voltage, Fermi energy is tuned to the centre of the moiré super lattice band gap (gap between first and second set of lowest energy bands), which manifests as the two prominent side peaks on either side of the charge neutrality point in resistance measurements. The number density that corresponds to the applied gate voltage (calculated for dielectric layers of SiO_2 thickness 285 nm and hBN thickness 18 nm) at the side peak position gives the superlattice carrier density n_s. Given the requirement of 4 electrons per moiré unit cell to fill or vacate the first moiré band, n_s. is denoted as band filling factor '$\nu = 4$ ' and the remaining band filling factors could be obtained converting number density (n) value to ν following the formula $4 * n/n_s$.

The twist angle was estimated using the relation, $n_s = 8\theta^2/\sqrt{3}a^2$, where $a = 0.246$ nm is the lattice constant of graphene . Furthermore, we note electron - hole asymmetry in the peak positions which has also been observed previously, [4, 7, 8]. We have mentioned error bars along with the twist angles in the manuscript, capturing the difference that could arise in the twist angle estimation because of the asymmetry in peak positions on electron and hole sides.

IV. TRANSPORT DATA FROM DIFFERENT MEASUREMENT CHANNELS

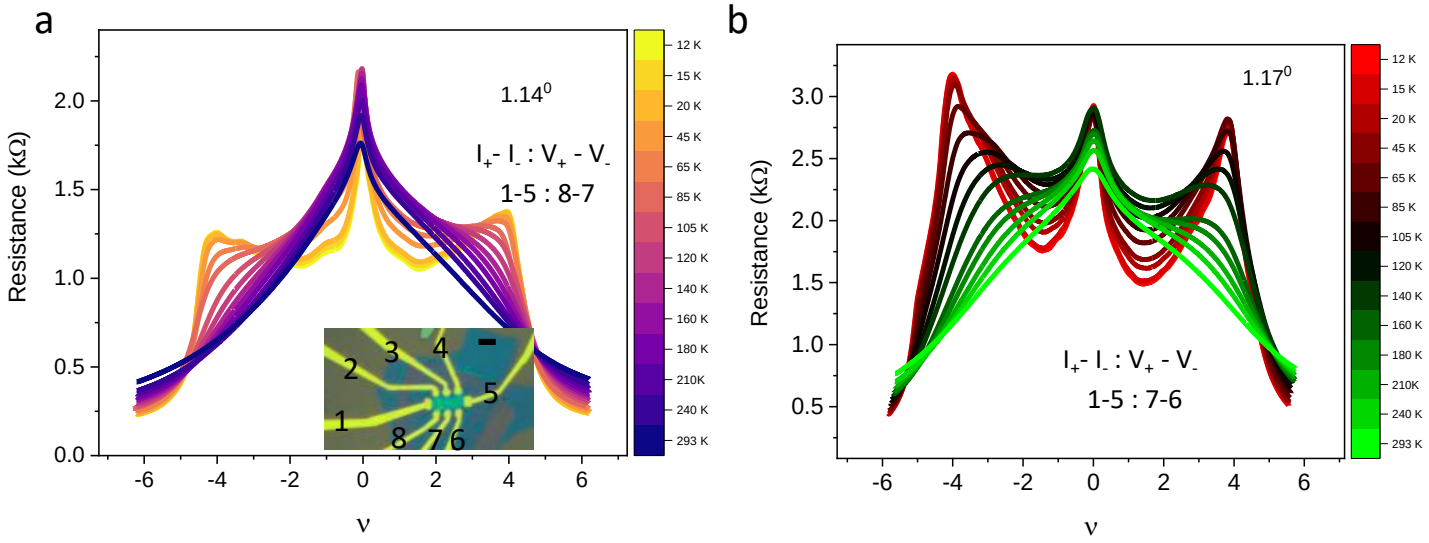

Fig. S2(a), (b) Four-probe resistance R as a function of filling ν measured at different temperatures between 12 K and 294 K for two different measurement channels with twist angle $\theta \approx 1.17^\circ \pm 0.02$ and $\theta \approx 1.14^\circ \pm 0.02$. The optical microscopic image and corresponding contact configuration is shown in the inset of **(a)** The scale bar represents a length of 2 μm. Both channels show insulating behaviour at $\nu = \pm 4$ and metallic behaviour in the intermediate density regime between $\nu = \pm 4$ and the Charge neutrality point (CNP) through out the measured temperature window.

V. PHOTORESPONSE DATA FROM DIFFERENT MEASUREMENT CHANNEL

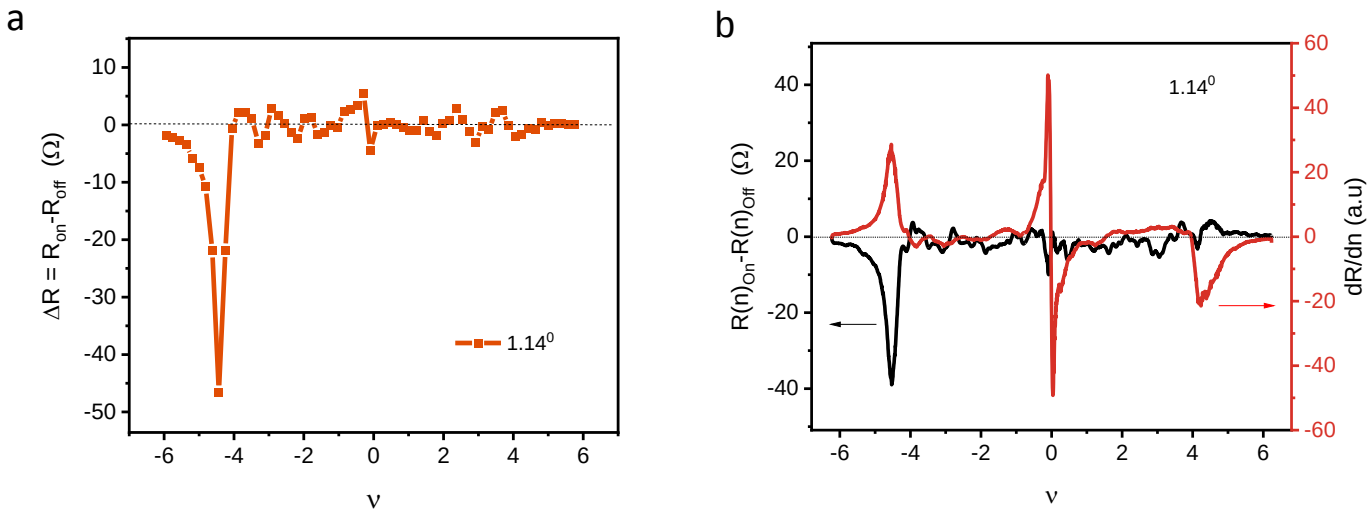

Fig. S3. Gate voltage dependence of the photoresponse from measurement channel with twist angle $\theta \approx 1.14^\circ \pm 0.02$ **a.** Photo resistance $\Delta R = R_{\mathrm{ON}} - R_{\mathrm{OFF}}$ as a function of ν **b.** Comparison between $R(n)_{\mathrm{ON}} - R(n)_{\mathrm{OFF}}$ (left axis) and dR/dn (right axis). The suppression of photoresponse below moiré band edge is verified irrespective of the prominent dR/dn peak at the CNP.

VI. PHOTORESPONSE MEASUREMENTS ON CONTROL DEVICE

In order to confirm that the observed photoresponse behavior is unique to tBLG, we perform photoresponse measurement on a WSe_2/bilayer graphene heterostructure-based device (Fig.S4). We note that the photoresponse follows dR/dV_{BG} magnitude, and the sign is determined by the direction of the applied gate field. As we observe photoresponse over the entire measurement gate voltage window, the suppressed photoresponse in tBLG/WSe_2 based device is confirmed to arise from the unique band structure of tBLG.

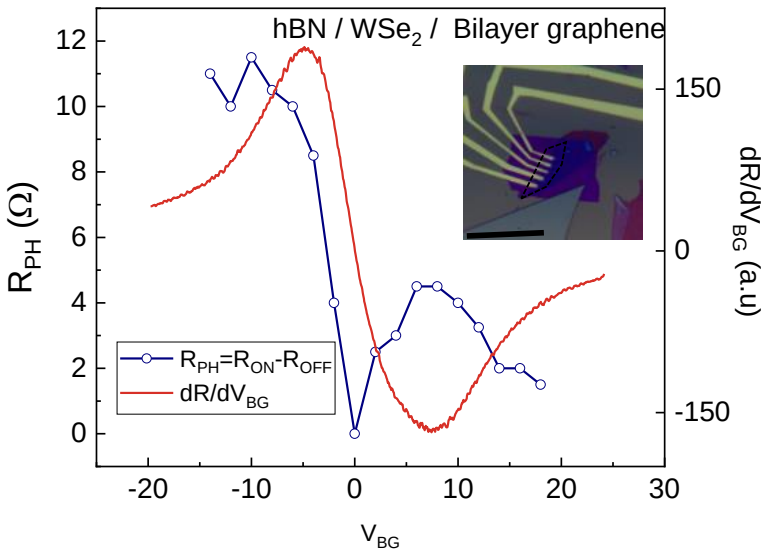

Fig. S4. Comparison between photoresponse and (left axis) and dR/dV_{BG} (right axis) in bilayer graphene based device. The photoresponse follows dR/dV_{BG} with the sign determined by applied gate electric field direction. Scale bar corresponds to 15 μm

VII. CONDUCTION BAND THRESHOLD OF WSe_2

Using the data present in references [9–12], we show the band alignment of tBLG and WSe_2 schematically in Fig. S5. At -15 V (where the resistance recovers back to its pre-illumination dark state), the Fermi level lies inside the valence band of tBLG and is expected to be $10-15$ meV below the CNP, which will remain far away from the conduction threshold of WSe_2. Although the exfoliated WSe_2 may be doped heavily, this possibility is disregarded because 1). such a large difference in the Fermi level should have resulted in large electron doping in tBLG. However, from the transport measurement, we observe that the CNP is around 1 V suggesting the low-hole doping in the system. 2). The WSe_2 crystals used here were purchased from 2D Semiconductors where the maximum expected doping density is less than $10^{10}/\text{cm}^2$. Thus it is safe to say that the charge distribution equilibrates throughout the hybrid due to the screening effects as the Fermi level is tuned deep inside the band and not because of the onset of the conduction band threshold of WSe_2.

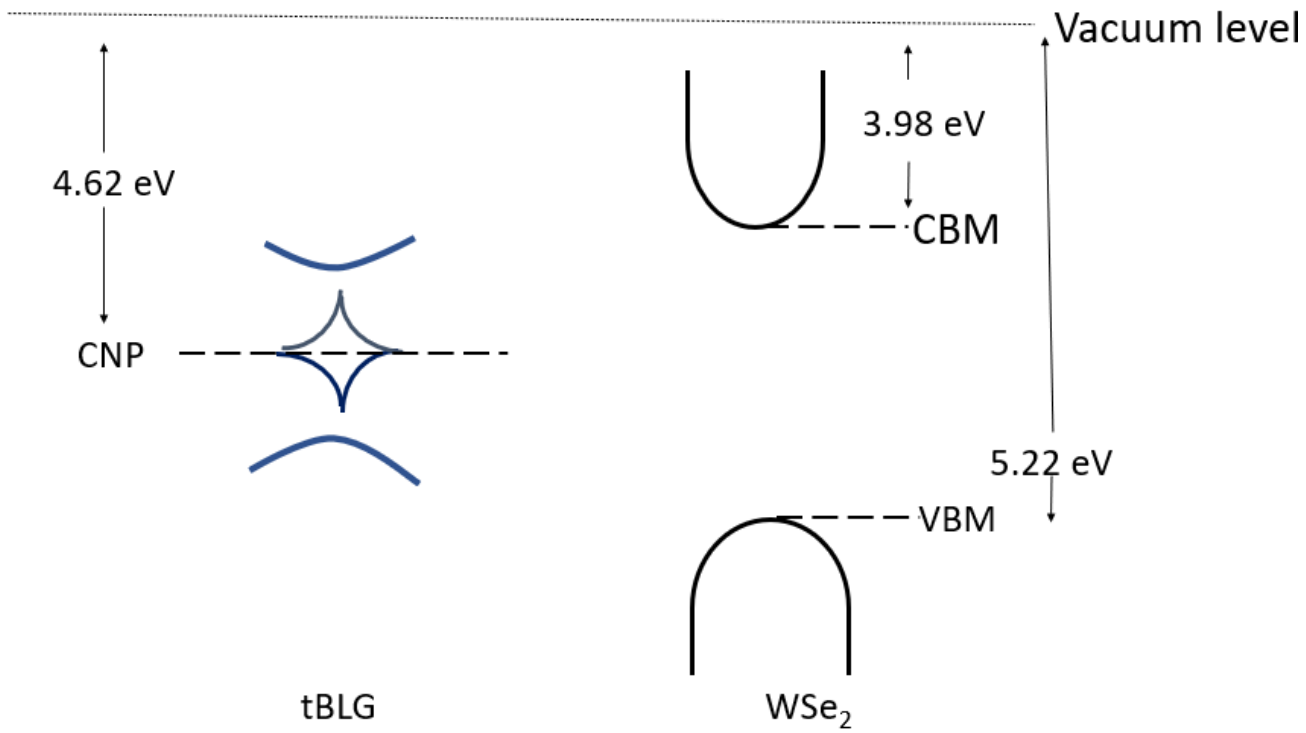

Fig. S5. The of band alignment of tBLG and WSe_2 is presented following reference [9–12]

VIII. PHOTRESPONSE AND dR/dn MAGNITUDE VARIATION AS A FUNCTION OF TEMPERATURE

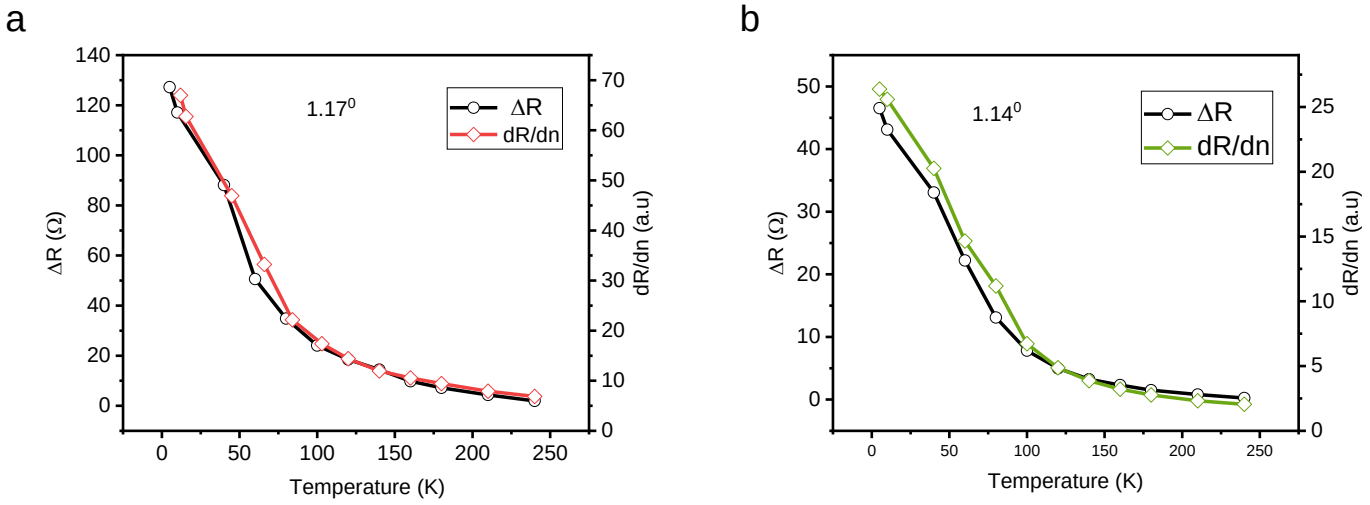

Fig. S6(a), (b). The variation of photoresponse magnitude at $\nu = -4.12$ is compared with that of of dR/dn at the same number density. For both the channels we observe the photoresponse following temperature dependence of dR/dn.

IX. PHOTORESPONSE AND dR/dn COMPARISON AT HIGHER TEMPERATURE

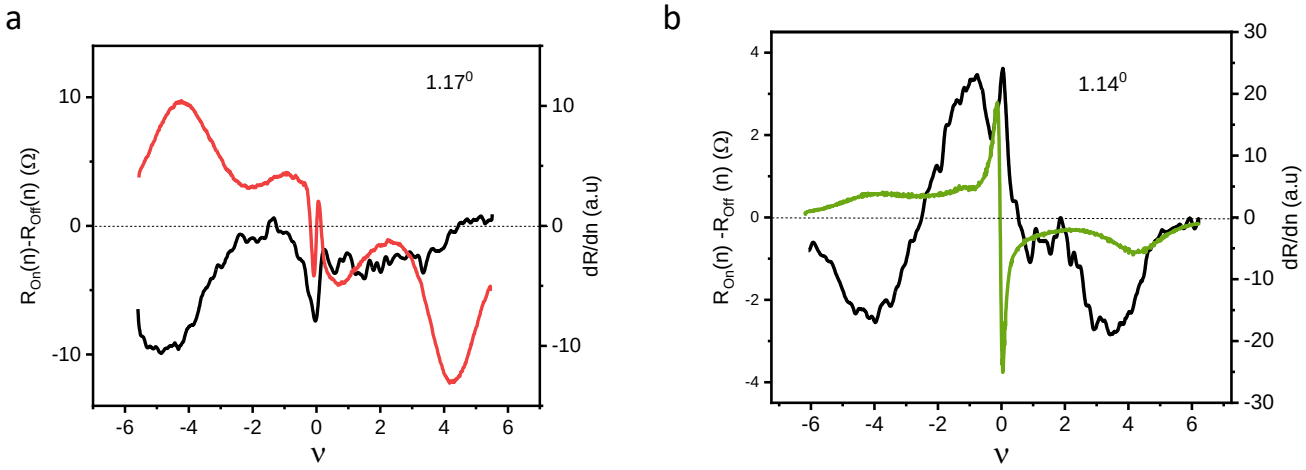

Fig. S7 (a), (b). Comparison between $R(n)_{\mathrm{ON}} - R(n)_{\mathrm{OFF}}$ (left axis) and dR/dn (right axis) at 160 K for two different measurement channels. a) A clear deviation from dR/dn is observed in photoresponse in conduction band. b) Deviation in photoresponse from dR/dn is prominent through out the measured window.

At higher temperatures, we observe a deviation in photoresponse from dR/dn at lower energies of the conduction band (Fig. S5). Conductance in tBLG being highly sensitive to temperature effects[13, 14], this observation opens up the possibility of exploring bolometric effect in this type of device architecture. Following the references [14, 15] we note that there are two possible origins of bolometric response in the device. 1) Direct electron and hole gas heating of tBLG upon infrared illumination as demonstrated by Hubmann et al. in reference [13] and 2) The energy transfer from optically excited TMDC to graphene as demonstrated by Majumdar et al.in reference [14]. As the observed photoresponse is restricted to above WSe_2 bandgap excitation, the bolometric effect from direct heating of tBLG is disregarded. Neither the contribution from heat transfer mediated photoresponse is captured at low temperature since the photogating dominates the response. However, at higher temperatures, as we note the deviation from the photogating trend, bolometric contribution arising from energy transfer along with charge transfer (possibly a hot carrier transfer) is considered. We believe that, at high temperature,

with the reduction in dR/dn magnitude (hence the photogating response), the bolometric contribution becomes relevant as the overall magnitude of the response at higher temperature is limited to $< 10\ \Omega$. As shown in ref [14, 15], such effects are extremely sensitive to interface coupling of different layers, and experiments involving Johnson noise thermometry could be explored in future to exactly quantify the respective contributions of photogating, lattice heating and electronic heating in this type of device architecture.

X. VARIATION OF PHOTORESPONSIVITY WITH OPTICAL POWER DENSITY

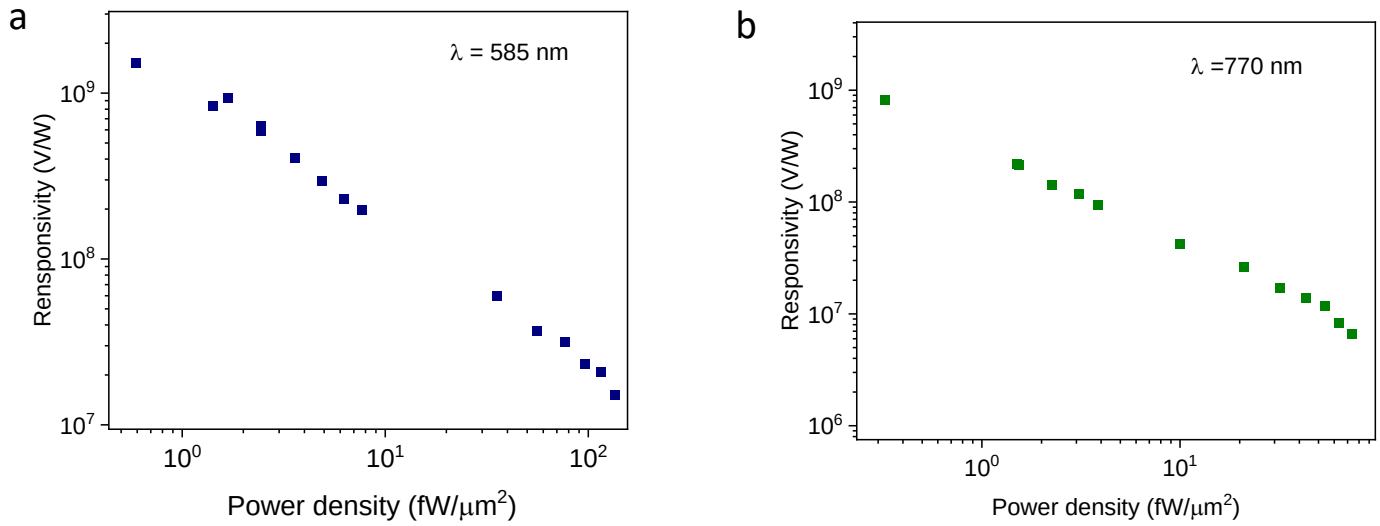

Fig. S8 (a), (b). Optical power density dependence of photoresponsivity at $|\nu| = -4.12$ for wavelengths a) 585 nm and b) 770 nm.

* aparnap@iisc.ac.in
† arindam@iisc.ac.in

[1] Xu, K. *et al.* Atomic-layer triangular wse2 sheets: synthesis and layer-dependent photoluminescence property. *Nanotechnology* **24**, 465705 (2013).
[2] Fang, H. *et al.* High-performance single layered wse2 p-fets with chemically doped contacts. *Nano letters* **12**, 3788–3792 (2012).
[3] Zhao, W. *et al.* Evolution of electronic structure in atomically thin sheets of ws2 and wse2. *ACS nano* **7**, 791–797 (2013).
[4] Cao, Y. *et al.* Correlated insulator behaviour at half-filling in magic-angle graphene superlattices. *Nature* **556**, 80 (2018).
[5] Bistritzer, R. & MacDonald, A. H. Moiré bands in twisted double-layer graphene. *Proceedings of the National Academy of Sciences* **108**, 12233–12237 (2011).
[6] Tarnopolsky, G., Kruchkov, A. J. & Vishwanath, A. Origin of magic angles in twisted bilayer graphene. *Physical review letters* **122**, 106405 (2019).
[7] Arora, H. S. *et al.* Superconductivity in metallic twisted bilayer graphene stabilized by wse2. *Nature* **583**, 379–384 (2020).
[8] Cao, Y. *et al.* Superlattice-induced insulating states and valley-protected orbits in twisted bilayer graphene. *Physical review letters* **117**, 116804 (2016).
[9] Ooi, N., Rairkar, A. & Adams, J. B. Density functional study of graphite bulk and surface properties. *Carbon* **44**, 231–242 (2006).
[10] Sque, S. J., Jones, R. & Briddon, P. R. The transfer doping of graphite and graphene. *physica status solidi (a)* **204**, 3078–3084 (2007).
[11] Yu, Y.-J. *et al.* Tuning the graphene work function by electric field effect. *Nano letters* **9**, 3430–3434 (2009).
[12] Pudasaini, P. R. *et al.* High-performance multilayer wse2 field-effect transistors with carrier type control. *Nano Research* **11**, 722–730 (2018).
[13] Hubmann, S. *et al.* Infrared photoresistance as a sensitive probe of electronic transport in twisted bilayer graphene. *arXiv preprint arXiv:2207.14223* (2022).
[14] Majumdar, A. *et al.* Probing the charge and heat transfer channels in optically excited graphene—transition metal dichalcogenide hybrids using johnson noise thermometry. *Applied Physics Letters* **121**, 041103 (2022).
[15] Froehlicher, G., Lorchat, E. & Berciaud, S. Charge versus energy transfer in atomically thin graphene-transition metal dichalcogenide van der waals heterostructures. *Physical Review X* **8**, 011007 (2018).